#### **ORIGINAL PAPER**



### Concurrent n-scale modeling for non-orthogonal woven composite

Jiaying Gao<sup>1</sup> · Satyajit Mojumder<sup>2</sup> · Weizhao Zhang<sup>1,3</sup> · Hengyang Li<sup>1</sup> · Derick Suarez<sup>1</sup> · Chunwang He<sup>1</sup> · Jian Cao<sup>1</sup> · Wing Kam Liu<sup>1</sup>

© The Author(s), under exclusive licence to Springer-Verlag GmbH Germany, part of Springer Nature 2022

#### **Abstract**

Concurrent analysis of composite materials can provide the interaction among scales for better composite design, analysis, and performance prediction. A data-driven concurrent n-scale modeling approach (FExSCA<sup>n-1</sup>) is adopted in this paper for woven composites utilizing a mechanistic reduced order model (ROM) called Self-consistent Clustering Analysis (SCA). We demonstrated this concurrent multiscale modeling theory with a FExSCA<sup>2</sup> approach to study the 3-scale woven carbon fiber reinforced polymer (CFRP) laminate structure. FExSCA<sup>2</sup> significantly reduced expensive 3D nested composite representative volume element (RVE) computation for woven and unidirectional (UD) composite structures by developing a material database. The modeling procedure is established by integrating the material database into a woven CFRP structural numerical model, formulating a concurrent 3-scale modeling framework. This framework provides an accurate prediction for the structural performance (e.g., nonlinear structural behavior under tensile load), as well as the woven and UD physics field evolution. The concurrent modeling results are validated against physical tests that link structural performance to the basic material microstructures. The proposed methodology provides a comprehensive predictive modeling procedure applicable to general composite materials aiming to reduce laborious experiments needed.

Keywords Virtual testing · Reduced order modeling · Concurrent modeling · Unidirectional and woven composite

#### 1 Introduction

Numerical methods have been developed in the past few decades to facilitate modeling and simulations of engineering materials systems. For example, Finite Element Analysis (FEA) for vehicle crash simulation has become a standard procedure in major vehicle manufacturers to virtually examine vehicle safety under various scenarios. Numerical models can reduce physical experiments needed and pro-

Wing Kam Liu w-liu@northwestern.edu
Satyajit Mojumder satyajitmojumder2022@u.northwestern.edu

Published online: 18 June 2022

- Department of Mechanical Engineering, Northwestern University, 2145 Sheridan Road, Tech B224, Evanston IL 60208-3109, USA
- Theoretical and Applied Mechanics Program, Northwestern University, 2145 Sheridan Road, Tech B224, Evanston IL 60208-3109, USA
- Present Address: Department of Mechanical and Automation Engineering, The Chinese University of Hong Kong, Shatin, N.T., Hong Kong SAR, China

vide significant savings in time and resources during the product development process. However, material physics linked into multiple length scales need to be considered to properly model the materials system through any numerical procedure. Concurrent multiscale modeling provides the interaction among material length scales that is crucial to incorporate material physics and build a thorough understanding of the materials system.

Composite materials are in general composed of at least two different phases. For example, the cured unidirectional (UD) carbon fiber reinforced polymer (CFRP) is made of continuous carbon fibers and polymer matrix. Prediction of UD CFRP properties can be carried out using a UD microstructure model (usually a representative volume element (RVE)) for numerical homogenization that is typically performed through FE or Fast Fourier Transformation (FFT) methods. Various UD CFRP properties, the elastic, elastoplastic, as well as the damage behavior of composites, can be predicted by the RVE model [1–6]. RVE analysis provides a good estimation of composite material constants and can be used for hierarchical multiscale modeling where the RVE output serves as the material law for the structural level model



[7,8]. Such an approach applies to woven composites as well, as seen in [9–11]. In the macroscale woven laminate, material properties can be approximated with mesoscale woven RVEs, and in each woven RVE, the yarn phase material properties can be approximated with microscale UD RVEs as each yarn is a mixture of many carbon fibers and epoxy matrix. Building a hierarchical multiscale model would allow one to incorporate mesostructure and microstructure elastic constants into the woven laminate [8,12,13], and hence evaluate laminate performance with homogenized information, yet such approach implies simplification on the nonlinear material behaviors.

For accurate prediction of engineering structures, one needs to establish the capability of efficient computation of CFRP nonlinear material responses. This requires the development of reduced-order modeling methods so the RVE model can be effectively embedded into the structural level model [14–17]. Composite concurrent multiscale modeling is established based on a reduced order modeling approach. Under the concurrent modeling framework, an RVE is replaced by a compressed RVE database, to substitute traditional material law approach in composite structural performance prediction. Two-scale (2-scale) concurrent modeling for UD and woven composites has been developed utilizing Self-consistent Cluster Analysis (SCA), a mechanistic reduced order modeling method, as reported in [18,19]. However, for 2-scale woven multiscale modeling, yarn properties are usually assumed to be linear elastic [4,12,18]. In this paper, a three-scale (3-scale) concurrent multiscale modeling approach, FExSCA<sup>2</sup>, is proposed in order to properly capture yarn plasticity (which is approximated using UD RVEs) during the woven structure deformation process. The outcomes are two-folded: (1) the prediction accuracy is improved by incorporating previously ignored physics, and (2) the history of the plastic strain accumulation in the woven and UD scale is recorded for a better understanding of microstructure evolution. While a 2-scale model is computationally preferred over a 3-scale model, a 3-scale model can provide further information on microstructure evolution of individual material phases (namely fiber and matrix for a single yarn in a woven composite). For a 2-scale model, the required calibration effort to characterize a woven RVE is high as one has to perform sizable physical testing such as tensile, shear, and compression tests at that level. Meanwhile, a 3-scale model only requires calibration on the constituents' material phases (fiber and matrix in this case), which is much more affordable from the experiment point of view [20].

From the above discussion, clearly there is a need for more than 2-scales in multiscale modeling to properly capture the relevant physics of lower scales. However, there exist challenges on computational efficiency on solving such large problems. Therefore, to address the challenge of solving

multiscale problems with greater computational efficiency, a data-driven reduced order computational framework is presented with examples of woven composites. The outline of the paper is as follows: Sect. 2 provides materials and methods for experimental woven bias-extension sample tests. Sect. 3 provides a concurrent n-scale modeling theory for heterogeneous materials using a mechanistic reduced order model. A 3-scale model for a 3-point bending test is presented in Sect. 4. Sect. 5 describes the concurrent multiscale modeling setup for cured woven tensile samples. Sect. 6 presents key simulation results, findings, and comparisons with experimental data for the cured woven tensile coupon. Sect. 7 concludes the paper with possible future directions.

#### 2 Materials and methods

### 2.1 Materials and sample geometry

In this work, bias extension tests are performed on cured woven prepregs with 60° yarn angle. First, woven prepregs with 90° yarn angle from Dow Chemical are used to manufacture the 60° non-orthogonal samples. Bias extension tests are performed on the orthogonal prepregs to generate shear deformation in order to achieve a 60° yarn angle. The bias-extension tests are performed at elevated temperature to reduce the resistance of uncured resin during shear deformation. The woven prepregs are trimmed and have an initial length that is at least twice the sample width. The prepregs with 60° yarn angles are then cured to make tensile test samples. The cured woven samples have overall fiber volume fractions between 44% and 48% per measurements done according to ASTM standard D792-01[21]. The 60° varn angle and the shape of the cured woven sample are visualized in Fig. 1. Detailed information on performing bias-extension tests and the curing process can be found in [11].

### 2.2 Experimental setup

Tensile tests are performed using a hydraulic testing machine with a load cell capacity of 100 kN. The cured woven samples are loaded on the testing machine, clamped on top and bottom ends, and deformed along the y axis denoted in Fig. 1. Axial strain is recorded by the strain gauge, and the axial loading force is recorded by the load cell. The data gathered from the tensile tests are used to generate the force vs. axial strain plots that are used for validation purposes. The tensile test is performed on three samples to ensure repeatability and quality of the force-strain curves.



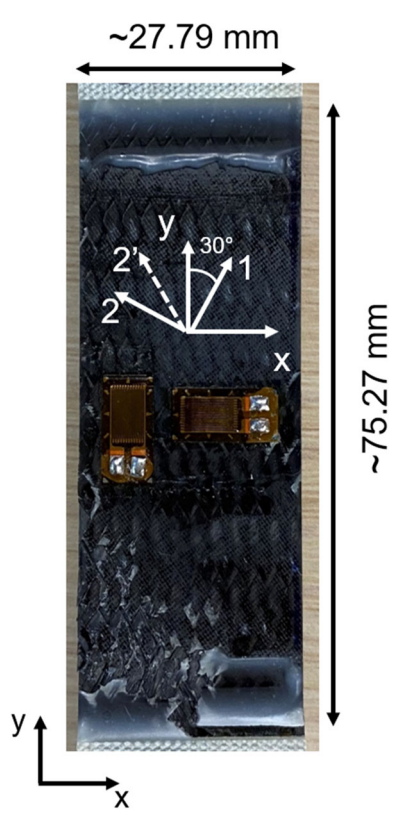


Fig. 1 The cured woven bias-extension sample (clamping region hidden) after testing, as seen by broken epoxy matrix and exposed yarns. 1 and 2 represent weft and warp yarns for the orthogonal configuration,  $90^{\circ}$  yarn angle. The sample has a tailored yarn angle of  $60^{\circ}$  represented by 1 and  $2^{\prime}$ 

#### 2.3 Computational model development

The woven composite structure is a good demonstration of the length scales of composite materials. To model a woven composite structure, we first took a 3-point bending woven composite laminate and attempt to develop a computational framework that can be applicable to the woven tensile sample. The computational complexity of 3-point bending of a woven composite laminate is shown in Fig. 2. Woven composite laminates can be modeled at part scale with multiple plies using FEA. Each material point of the laminate can be represented by a mesoscale woven RVE (4x4 twill here) having multiple yarns. A zoomed in view of the yarn reveals a UD structure at the microscale. To fully model the laminate concurrently, one would need to solve approximately  $10^{18}$  degrees of freedom (as shown in the figure), which is not computationally feasible. Therefore, an efficient multiscale theory is required to model multiple scales together. Utilizing the data-driven techniques of mechanistic reduce order modeling, this problem becomes tractable with a desktop computer. This type of multiscale model is necessary to properly capture the materials physics at multiple length scales. Solely using a 2-scale model for the woven composite laminate is not able to consider the plasticity from the UD yarn structure. Moreover, the overall fiber volume fractions can be captured more accurately if more scales are considered.

## 3 Concurrent theory for n-scale materials modeling

#### 3.1 General n-scale theory

Composites are heterogeneous materials with multiple length scales. Fig. 3 shows a composite material system with *n* number of scales. Each scale has heterogeneity that can be further analyzed in a finer scale as shown in the figure. This general multiscale boundary value problem can be expressed using the equilibrium, compatibility equations with necessary boundary conditions and material law as given in Eq. 1 for n-scales.

$$\begin{cases} \nabla \cdot \boldsymbol{\sigma}^{1} + \boldsymbol{b}^{1} = 0, & in \ \Omega^{1} \\ \boldsymbol{t} = \bar{\boldsymbol{t}}, & on \ \partial \Omega_{t}^{1} \\ \boldsymbol{u} = \bar{\boldsymbol{u}}, & on \ \partial \Omega_{u}^{1} \\ \boldsymbol{\sigma}^{n}(\boldsymbol{X}^{n}) = \begin{cases} \frac{1}{\Omega^{n+1}} \int_{\Omega^{n+1}} \boldsymbol{\sigma}^{n+1}(\boldsymbol{X}^{n+1}) \Omega^{n+1}, \\ & if \ \boldsymbol{X}^{n} \ has \ microstructure, \ n = 2, ..., N \\ f^{n}(\boldsymbol{\varepsilon}^{n}), & n = 1 \\ \nabla \cdot \boldsymbol{\sigma}^{n} = 0, \ n = 2, ..., N \\ \boldsymbol{\varepsilon}^{n}(\boldsymbol{X}^{n}) = \frac{1}{2} (\nabla \boldsymbol{u}^{n}(\boldsymbol{X}^{n}) + (\nabla \boldsymbol{u}^{n}(\boldsymbol{X}^{n}))^{T}), \forall \boldsymbol{X}^{n} \in \Omega^{n}, \ n = 2, 3, ..., N \end{cases}$$

$$(1)$$

where  $\sigma^1$  is the macroscale stress tensor and  $b^1$  is the macroscale body force, t and u are the applied Dirichlet boundary conditions, and  $\sigma^n(X^n)$  and  $\varepsilon^n(X^n)$  are stress and strain tensors at each lower scale n integration point  $X^n$ .

In equation set 1, the first three equations describe the macroscopic problem, where Dirichlet boundary conditions are applied to define displacement or the applied force at the boundaries of the structure. The fourth equation defines the constitutive behavior for material points in scale n. If microstructure information needs to be captured, mean field homogenization is applied on scale n+1 to obtain effective stress responses for scale n. If microstructure is not needed, then the standard material constitutive law can be applied on n. For finer scales where n>1, microstructure responses are resolved assuming periodic displacement field and antiperiodic traction boundary condition, as described by the last two equations in Eq. 1. Details on the solution approach are provided in 1, and interested readers are referred to [22] and [14] for further discussions.

Most modern engineering applications, such as vehicle crash simulations, are modeled at the macro or part scale. Finite Element Method (FEM) can be applied to solve



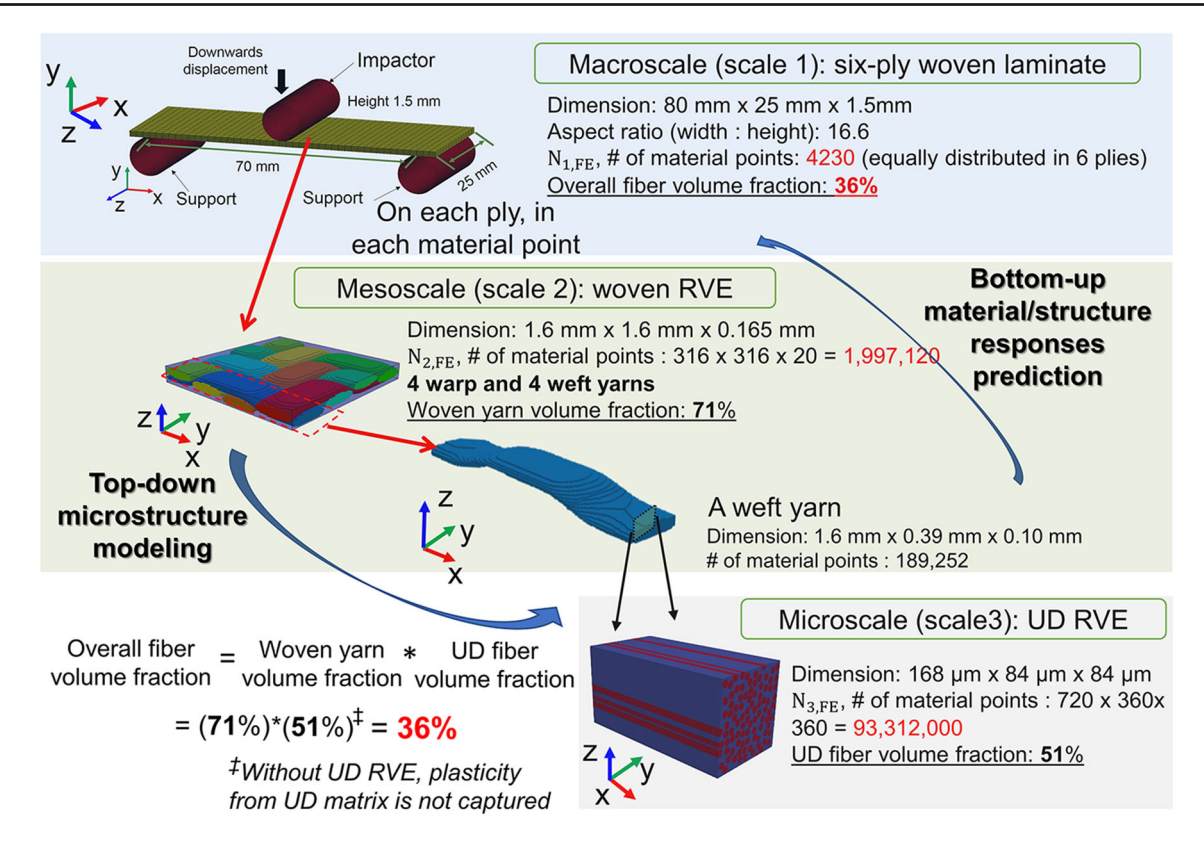


**Fig. 2** Macroscale FE model of a woven laminate under 3-point bending is shown on the top panel. Each material point in the macroscale laminate is represented by a mesoscale woven RVE shown in the middle panel, and a material point in the yarns (weft yarn shown) is represented

by a microscale UD RVE shown in the bottom panel. An estimate of the overall fiber volume fraction captured through these three scales is shown

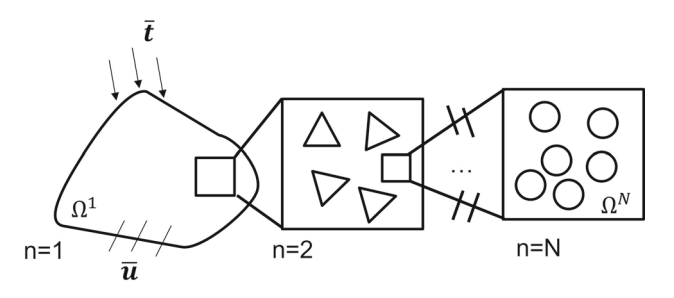


Fig. 3 A general illustration of the N-scale multiscale problem. n=1 is the macroscale, and n>1 are finer scales representing the underneath heterogeneity [22]

macroscale problems easily due to its generality in describing complex geometries [23–25]. Other methods, such as Isogeometric Analysis [26,27] and meshfree methods [28–30] are also applicable. However, a one-scale analysis means microstructure information cannot be directly captured, and that the simulation process requires effective material laws [31]. Applying a concurrent multiscale approach can capture lower scales physics such as damage evolution, among others, which makes the part-scale prediction more accurate.

#### 3.2 Reduced order model for concurrent analysis

From the general concurrent n-scale equations presented in Eq. 1, each scale needs to be solved simultaneously. As shown in Fig. 2, considering three scales requires solving approximately 10<sup>18</sup> degrees of freedom, which is not computationally feasible. At each lower scale, RVE responses are evaluated assuming periodic boundary conditions to ensure convergence by alleviating the size effect. Each mesoscale and microscale RVE are given an effective strain increment during the concurrent analysis. The RVE model then computes its effective RVE stress increment using a numerical homogenization technique, such as FFT. The effective stress increment is passed back to the higher scale in order to continue the concurrent analysis. However, direct RVE calculation is very expensive, as each RVE contains millions of voxel elements. To counteract this issue, a mechanistic reduced order modeling method, Self-consistent Clustering Analysis (SCA) [14], is leveraged. Details of the method are given in 1. Reduced-order models (ROMs) of RVEs are built to replace original high fidelity RVEs as shown in Fig. 4. The ROMs are built using a high performance computing (HPC) cluster - computing node equipped with 24 cores at 2.5 GHz



 Table 1
 Elastic material constants for fiber (transversely isotropic elastic) and epoxy (isotropic elastic)

Fiber	Values	Matrix	Values
$\overline{E_{11}}$	245 GPa	E	3.8 GPa
$E_{22} = E_{33}$	19.8 GPa	ν	0.39
$G_{12}=G_{13}$	29.2 GPa		
$G_{23}$	5.92 GPa		
$v_{12} = v_{13}$	0.28		
v <sub>23</sub>	0.32		

and maximum random-access memory of 64 GB. The UD RVE computation takes 12 hrs for the elastic responses, 0.25 hr for the K-means clustering, and 2 hrs for computing the interaction tensor. The woven RVE computation takes 3 hrs for the elastic responses, 0.1 hr for the K-means clustering, and 0.06 hr for computing the interaction tensors.

### 4 3-scale model setup for 3-point bending test of a woven laminate

A common material testing procedure for determining the structural level properties under combined loading of composites laminates is the flexural test. The flexural test can be performed either as a 3-point or 4-point bending test [32,33]. The flexural test can be used to investigate the elastic response of the composite laminate (such as flexural modulus), as well as the flexural strength if needed. To perform the virtual 3point bending test, a macroscale woven laminate model is constructed. The 3-point bending test woven laminate structure is adopted from [33], depicted in Fig. 2. The laminate has a length of 80 mm (70 mm between two rigid supports), a width of 25 mm, and a thickness of 1.5 mm. The two circular supports have diameters of 10 mm, separated 70 mm apart from each other, as shown in the Macroscale section of Fig. 2. A loading nose or impactor of equal size as the two supports pushes the laminate downwards in the negative y direction. Carbon fiber and epoxy material properties are given in Table 1, though epoxy plasticity is not considered as the purpose of the test is to investigate the flexural modulus of the laminate structure.

In the concurrent model, the woven laminate is considered the macroscale. One material point of the macroscale laminate is modeled with a woven RVE at the mesoscale. The mesoscale woven RVE is depicted in Fig. 5 a), with a yarn width of 0.39 mm, length of 1.6 mm, and thickness of 0.165 mm. The woven yarn volume fraction is 71%. The woven RVE containing 1,997,120 voxel elements is replaced by a ROM containing 4 clusters for the matrix phase and 16 clusters for the yarn phase. A fiber volume fraction of 51% is assumed for the yarn phase, and each cluster of the yarn

phase is represented by a microscale UD RVE depicted in Fig. 5 b). The UD RVE containing 93,312,000 elements is replaced by a ROM that has 4 clusters for the matrix phase and 2 clusters for the fiber phase. It is worth noting that the SCA ROM is not limited to two-phase materials (e.g., fiber and matrix) only. Any arbitrary number of phases can be included as an additional material phase in the RVE. For instance, the interphase among the fiber and matrix in a UD structure or a hybrid composite with more than one fiber can be modeled in such a fashion. Previous studies on UD CFRP [19] and filled rubber [34] have demonstrated such approach by adding the additional material phase, which can be easily extended for the current study.

The information passed in the 3-point bending concurrent modeling simulation is given in Fig. 2. Under this setup, at each integration point in the laminate model, a woven ROM is used to compute the material response at that integration point. For all yarns in the woven ROM, UD ROMs are used to compute the yarn responses. The prediction of the flexural modulus is compared with the theoretical value, as shown in Table 2. The flexural modulus follows the equation given below [35]:

$$E = \frac{L^3 m}{4wh^3} \tag{2}$$

where m is the slope of the force-deflection curve computed from simulation, L is the length between two supports, and w and h are the width and height of the woven laminate. The theoretical value is computed from the woven RVE by applying loading along the local 1 (or 2) direction. Since the flexural modulus is one way to evaluate a woven laminate's tensile behavior, a good match is observed.

The flexural modulus represents only the macroscopic property of the woven laminate. Another important feature of the 3-scale concurrent model is to provide microstructure physical fields (such as von Mises stress) evolution in the mesoscale and microscale, as shown in 1. A movie for the concurrent evolution of the stress field in the 3-point bending sample and the RVEs at different scales is provided as Supplementary material (S1).

The 3-point bending example shows how 3-scale multiscale concurrent modeling can be used to predict both macroscopic flexural modulus and microstructure evolution. This establishes the baseline for conducting a virtual test for a woven laminate structure. For practical usage, realistic woven and UD microstructures can be used as input to provide a microstructure driven prediction of structural performance. Alongside structural performance, microstructure evolution can be used to identify weak spots in both the mesoscale and microscale, and guide further design iterations for enhancing structural performance and integrity. Such virtual design process reduces the number of experimental trials needed, and



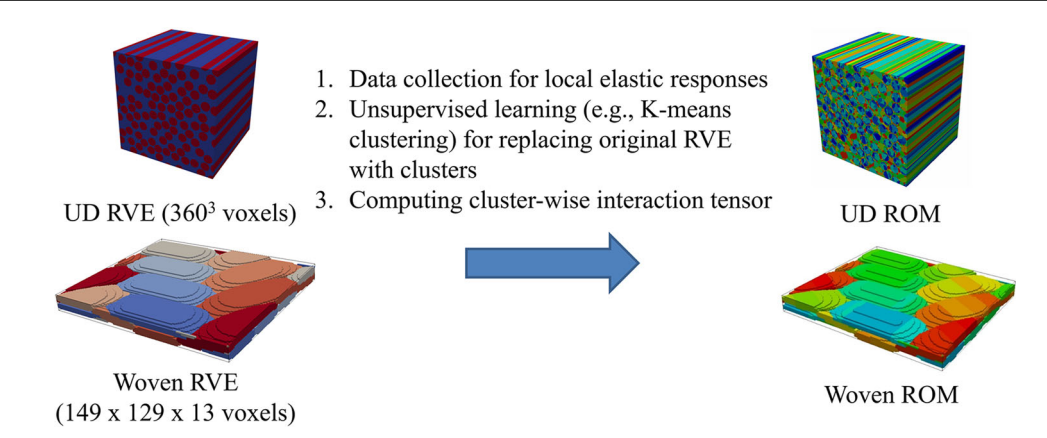


**Fig. 4** ROMs construction for UD and Woven RVEs, where voxel elements' boundary lines are hidden for clarity. Each RVE undergoes a three step data compression process (through unsupervised learning) in order to build the ROM. After the data compression process, the UD RVE is replaced with a ROM with 8 clusters (6 in the matrix phase and

2 in the fiber phase), and the woven RVE is replaced with a ROM with 40 clusters for the woven bias-extension tensile coupon modeling (8 in the matrix phase and 32 in the yarn phase). Same colored voxels belong to the same cluster within each ROM RVE

**Fig. 5** Geometric specification for a) woven RVE; b) UD RVE

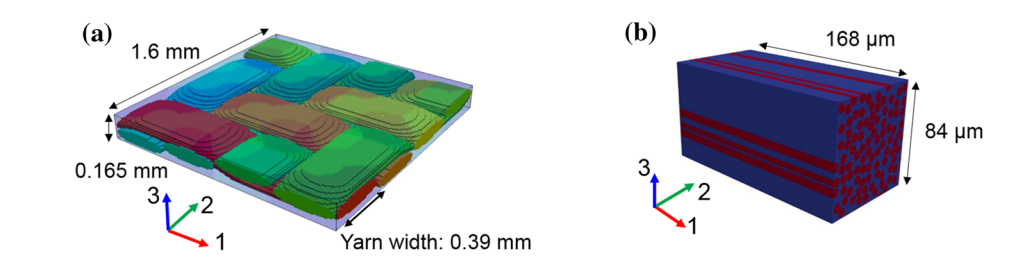


**Table 2** Comparison of theoretical (given by equation 2) and multiscale model prediction of flexural modulus

	Theoretical value	Multiscale model prediction	Difference
Flexural modulus	48.77 GPa	47.31 GPa	3.0%

provides a trustworthy approach for obtaining the structural performance of composites.

# 5 Concurrent modeling of cured woven tensile sample

In this section, the concurrent multiscale model development for the woven bias extension sample is described. The woven extension test sample is considered as a 3-scale problem where the macro scale is the sample itself, and meso- and micro-scale are the woven and UD composite scales, respectively, as shown in Fig. 4. The UD RVE is replaced with a ROM with 8 clusters (6 in the matrix phase and 2 in the fiber phase), and the woven RVE is replaced with a ROM with 40 clusters (8 in the matrix phase and 32 in the yarn phase). The macroscopic test sample itself is modeled with a single layer solid FE mesh at a resolution of 19 by 51 elements in the xy plane. Using a conventional pre-calibrated material model one can compute woven composites responses at each mate-

rial point for the macroscale model; however, ad-hoc nature of such models limit predictability.

In this work, instead of using a materials law for the woven structural analysis, woven RVEs are deployed at each material point which compute woven material responses on the fly. An important issue that needs to be addressed in the concurrent modeling of the woven composite is the yarn material properties. As the yarn phase is essentially a mixture of long fibers and epoxy matrix, it can be assumed to behave similarly to a UD composite. With this assumption, the yarn behavior can be computed using UD RVEs. Coupling the macroscale model, mesoscale woven RVEs, and microscale UD RVEs, one arrives at a 3-scale multiscale model for woven structures. This 3-scale model requires one to resolve several woven and UD RVEs. Such 3-scale concurrent model can be computationally prohibitive considering RVE models usually contain millions of integration points. Therefore, in the current work, we adopt a 3-scale concurrent multiscale modeling approach with a reduced order modeling method, FExSCA<sup>2</sup>, that alleviates the drastic computational cost brought by RVEs. Under this 3-scale concurrent scheme,



responses of all RVEs are evaluated during the deformation process of the tensile sample. In the modeling process, first we construct ROMs for the woven and UD RVE, and later these precomputed ROMs are used for concurrent analysis of the multiscale model. Note unless otherwise clarified, all microstructure RVEs are built for cured composite materials. Carbon fiber and epoxy matrix are considered for the materials and the properties are taken from Table 1. The epoxy matrix is assumed to have elasto-plastic behavior modeled with isotropic hardening following the yielding curve  $\bar{\sigma} = 30 + 50\bar{\epsilon}^{0.15}$ , stress unit in MPa. The hardening yielding curve is calibrated using Hollomon equation [36] against experimental tensile test data available for epoxy[37].

In the 3-scale concurrent model, the mesoscale model provides material responses in each macroscale material point. In a similar fashion, the microscale model provides material responses in each mesoscale yarn material point. Here, the mesoscale model and the microscale model are identified as the woven RVE and the UD RVE, respectively. Modeling of two RVEs lays down the foundation of 3-scale concurrent modeling.

The woven RVE model is constructed in TexGen [38]. As shown in Fig. 6 (a), the yarn width is defined as 0.36 mm. Four weft and four warp yarns are considered in the woven RVE model. The warp yarns are rotated 30° in the clockwise direction on the 1-2 plane to setup the 60° yarn angle (denoted by 1 and 2'). The overall thickness of the RVE is 0.12 mm, with a yarn volume fraction of 85%. The woven RVE contains 149 voxels along the 1 direction, 129 voxels along the 2 direction, and 13 voxels along the 3 direction. The woven RVE can be used to compute woven material behavior once the basic constitutive laws are integrated. Here the epoxy material is assumed to be isotropic with J2 plasticity following material properties given in Sect. 4 and hardening properties above. For the yarn phase, the microscale UD RVE model is needed in order to replace its constitutive law.

The UD RVE is generated following the methodology described in [19]. The methodology utilizes a Monte Carlo approach to pack a square domain with circles, forming the cross section of the UD RVE. The fiber volume fraction needs to be given in order to perform the packing procedure. In the physical woven sample preparation process, the overall carbon fiber volume fraction was measured to be between 44% and 48%. This means one needs to back-calculate the UD fiber volume fraction using the aforementioned numbers. Note that the overall fiber volume fraction is simply defined as the product of (fiber volume fraction in UD RVE)×(yarn volume fraction in woven RVE). Two UD RVEs are modeled with 51% and 56% fiber volume fractions. One of the UD RVEs is shown in Fig. 6(b). Each UD RVE contains 360³ voxels.

The overall 3-scale modeling framework is shown in Fig. 7, where the macroscopic material responses are pro-

vided by woven RVE with varn angle of 60°. In Fig. 7, the macroscale test sample is modeled as a FE model with the same geometric specifications as the real coupon. The upper side of the sample is pulled upwards (as denoted by the red arrow), and the bottom side is fixed in all directions. The FE model is constructed in LS-DYNA [39], and contains 19 elements in the x direction, 53 elements in the y direction, and 1 element in the z direction. The model is meshed with solid elements, and each element contains one integration point. At each integration point, its material responses are computed using a 60° woven RVE in the 3-scale concurrent multiscale modeling framework, as illustrated. Since the overall fiber volume fraction measured for the physical test samples was between 44% and 48%, two woven tensile 3-scale models are generated: one with overall fiber volume fraction of 44% and one with fiber volume fraction of 48%. Recalling that the overall fiber volume fraction is defined as the product of varn volume fraction and UD fiber volume fraction, this is done through fixing the varn volume fraction and assigning two different UD RVEs: one with 51% fiber volume fraction and one with 56% fiber volume fraction. These two cured woven tensile test models are expected to predict the lower bound and upper bound of the force vs. axial strain curves, forming a band that encompasses all experimental data.

#### 6 Results and discussion

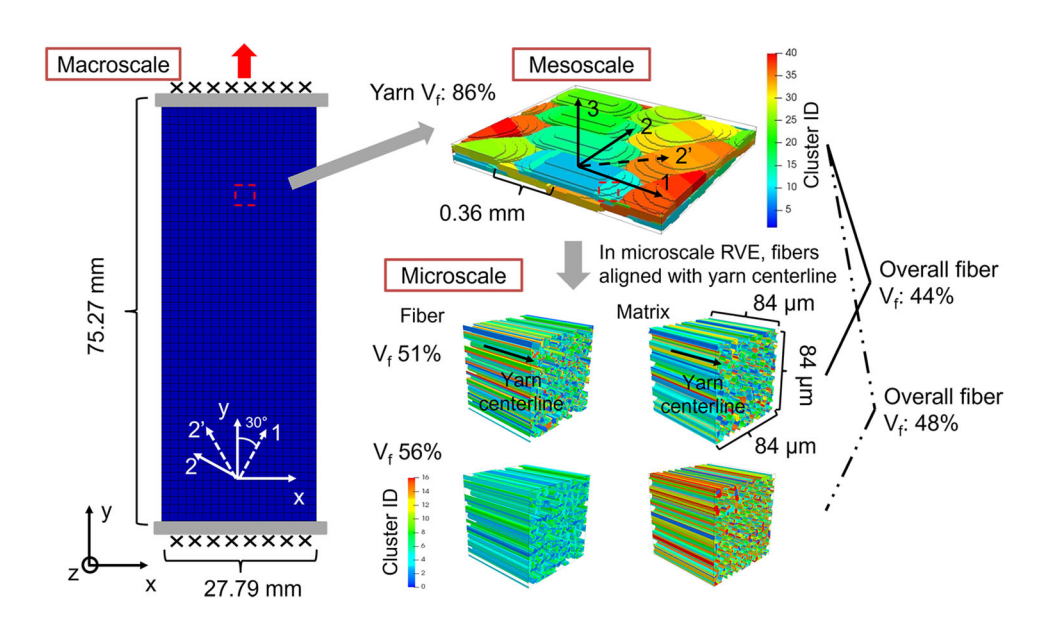
As described in the previous section a three-scale concurrent multiscale model, FExSCA<sup>2</sup>, is set up for the non-orthogonal woven bias extension sample. From the concurrent multiscale analysis in LS-DYNA, the loading force along the y direction and axial strain are outputted for the entire loading, to be compared with experimental data. The numerical prediction is plotted along with the experimental data obtained for three samples, identified as samples 1, 2, and 3. Those three samples all have the same geometry and are used to ensure the repeatability of the tensile test. As shown in Fig. 8, the three force vs. axial strain curves of the three tensile test samples show the same trend and are very close to each other, suggesting a good repeatability of the cured woven biasextension test. From the figure it is clear that considering UD microstructure to approximate yarn responses is necessary to properly match the experimental data. At this point, it has been shown that a UD RVE with only elastic material laws for the fiber and matrix can be used to compute the effective stiffness (an elastic property) of the UD RVE. In the 3-scale model, the UD RVE has a matrix phase with elastoplastic material behavior. Assuming the matrix phase in the UD RVE behaves elastically degenerates the 3-scale model to a 2-scale model. 2-scale and 3-scale concurrent multiscale simulations at 48% fiber volume fraction are performed, and the force vs. axial strain curve is also shown in Fig. 8.



**Fig. 6** (a) Mesoscale woven RVE with 60° yarn angle. The matrix phase is hidden for clarity so yarns can be observed. UD RVE with 44% fiber volume fraction. The dimension of the RVE is 84  $\mu$ m by 84  $\mu$ m by 84  $\mu$ m

84 μm 0.36 mm
(a)
(b)

Fig. 7 3-scale concurrent multiscale model for the cured 60° woven tensile test. The cluster distributions for mesoscale woven ROM of the woven RVE (yarn phase) and microscale UD ROM of the UD RVE(fiber and matrix phase) are depicted. Two different UD RVEs are used to capture sample fiber volume fraction upper and lower bounds



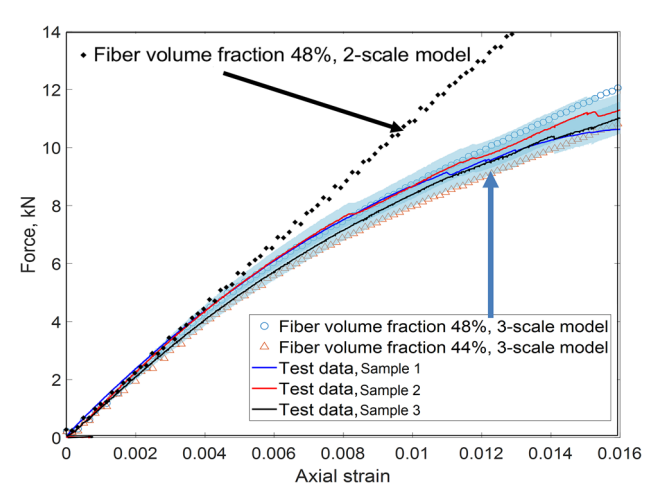


Fig. 8 Loading force vs. axial strain plots for 2-scale and 3-scale concurrent multiscale predictions and experimental data. The sample fails after 0.016 axial strain

The 3-scale prediction agrees well and captures the trend of the experimental data. However, the results from the 2-scale model, which ignores matrix plasticity, diverge drastically from the test data when the axial strain is larger than 0.004. The flat curve indicates that the 2-scale model behaves elastically throughout the entire virtual tensile test and fails to correctly predict the woven tensile sample response. The results suggest the matrix plasticity in the UD RVE matrix phase has a significant contribution to the nonlinear behavior of the woven tensile sample. Therefore, the 60° woven tensile sample has to be constructed using a 3-scale model so that the material responses can be properly captured. Two cured bias extension models are built in order to examine the effect of overall fiber volume fraction in the sample. The predictions made by the 3-scale model with 44% and 48% fiber volume fraction are visualized in Fig. 8. Both predictions agree well with the test data. To be specific, the sample with 48% draws the upper bound for the test data, and the sample with 44% draws the lower bound, successfully drawing a band that captures all three experimental data curves. The results suggest the present methodology can potentially replace partial experimental trial (constituent experimental data is all that is needed for the model), and provide a high quality prediction of woven composite responses (in this



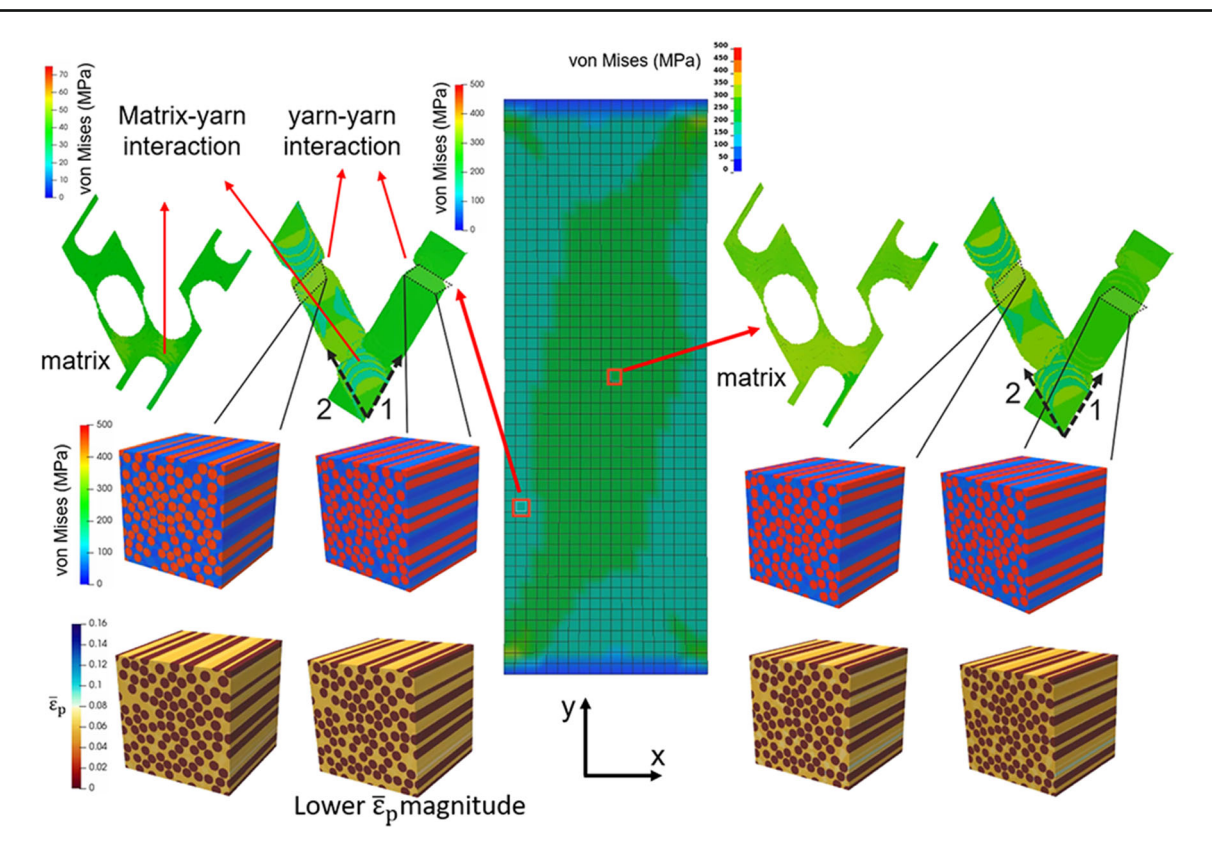


Fig. 9 Visualization at axial strain of 0.006: Cured woven bias-extension sample von Mises stress contour, mesoscale yarn and matrix von Mises stress contour, and microscale von Mises stress and effective plastic strain contours

case, tensile responses). Note that by utilizing UD RVEs at the lowest scale, the yarn behavior is computed on-the-fly and thus reducing certain calibration efforts compared to utilizing a phenomenological material law. Moreover, the UD RVEs provides a convenient way to store microstructure evolution on-the-fly that can be visualized as shown in Fig. 9 to Fig. 11, enabling observation of local stress and strain distributions. A movie for the concurrent evolution of the stress and strain field in the cured woven bias-extension sample and the RVE's at different scales is provided as Supplementary material (S2).

The deformed cured woven bias-extension simulation sample and the local yarn-UD plastic strain distributions are visualized in Figs. 9–11 at axial strains of 0.006, 0.01, and 0.016, respectively. In each figure, mesoscale woven RVEs at two boxed locations are visualized. For both woven RVEs, part of the woven RVE, including one weft and one warp yarns, is visualized in order to examine the local shear deformation. On each yarn, one integration point is picked out and its underneath UD RVE is visualized to examine the yarn plastic strain accumulation through out the entire deformation process.

In Fig. 9, the axial strain has reached 0.006 and one can see stress starts to concentrate in the middle due to 60° yarn angle.

There is a X shaped stress band in the sample, showing higher stress magnitude than the rest of the sample. The woven RVE in the stress concentration region is shown on the right of Fig. 9; its yarn and matrix phase both demonstrate higher stress magnitude than those from the woven RVE, shown on the left, outside the stress concentration region. Moreover, by taking cross sections of both yarns on two woven RVEs, microscale UD stress and effective plastic strain ( $\bar{\epsilon}_p$ ) evolution are revealed. The stress magnitude of UD RVEs shown right is higher than RVEs shown left, corroborating with the trend observed on the woven RVEs. The  $\bar{\epsilon}_p$  contour shows the UD RVE undergoes plastic deformation, which is the source of the nonlinearity observed in Fig. 8. In addition, the  $\bar{\epsilon}_p$  contours shown right show higher magnitude than contours shown left.

Figure 10 shows detailed evolution of those physical fields introduced in the previous figure once the axial strain reaches 0.01. Here, on the right the stress contours of the two UD RVEs are very close to each other, but the  $\bar{\varepsilon}_p$  contours suggest the UD RVE in the yarn along the 2 direction suffers larger deformation as shown by higher  $\bar{\varepsilon}_p$  magnitude. On the left, one can see the two UD RVEs have less  $\bar{\varepsilon}_p$  than those shown right. The difference in the stress contours for yarns along the 2 direction is less obvious. This suggests that the capture



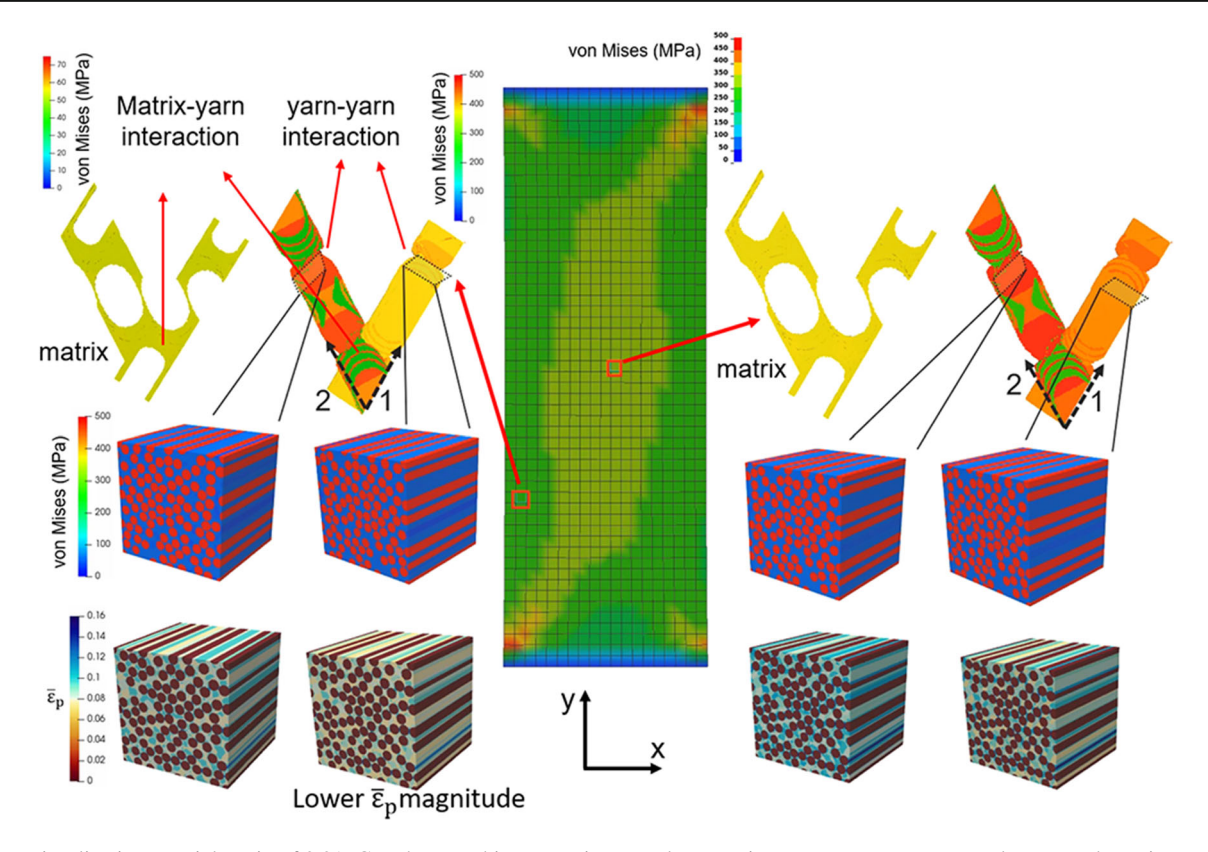


Fig. 10 Visualization at axial strain of 0.01: Cured woven bias-extension sample von Mises stress contour, mesoscale yarn and matrix von Mises stress contour, and microscale von Mises stress and effective plastic strain contours

of microscale  $\bar{\varepsilon}_p$  can play an important role in governing yarn failure, providing a possible alternative to stress-based failure criteria in the multiscale models.

Finally, as the axial strain reaches 0.016, Fig. 11 shows that the difference in woven RVE stress contours is almost negligible. However, the contrast in UD RVE  $\bar{\epsilon}_p$  can be used to quantify the difference. Most of the matrix phase on the right reaches  $\bar{\epsilon}_p$  of 0.16, while the matrix phase on the left shows  $\bar{\epsilon}_p$  of around 0.12, a 33% difference.

In terms of computational time, the study case shown here was performed on a HPC cluster using two nodes, each node having 24 processors. The entire computation takes 40 hours, and the physics over 969 woven RVEs (one in each macroscale integration point) and 15504 UD RVEs (one in each yarn cluster) are revealed simultaneously. Comparing to an estimated full scale model with a voxel mesh for woven and UD RVEs, the speedup achieved by the ROM is in the order of  $10^8$ .

To further accelerate the computational efficiency for large structures, the precomputed microstructure database can be leveraged. In a previous paper of the authors [7], the idea of estimating material microstructure behavior using Neural Networks (NN) is illustrated. This means there can be an offline stage where the material microstructure behav-

ior is pre-computed using ROMs under different loading conditions and load-paths, and NN are used to establish the material response, feeding the macroscopic FEM with the material responses. Since the NN evaluation is almost instantaneous, the computational cost can be further reduced, though this means all the microstructure evolution information cannot be stored on-the-fly during the macroscopic FE simulation.

The 3-scale bias extension model successfully reproduced the nonlinear stress and strain curve observed in experiments. The detailed physics revealed by the 3-scale model provides convenience in analyzing nonlinear behavior of the woven composite structure. Such details provided by the 3-scale model make it possible to capture local matrix plastic strain concentration in determining matrix failure. This concurrent multiscale tool can be useful for the design and analysis of different architectured composites such as woven and braided structures.

#### 7 Conclusion

In this paper, a 3-scale concurrent multiscale modeling theory is adopted with a demonstration of a woven composite



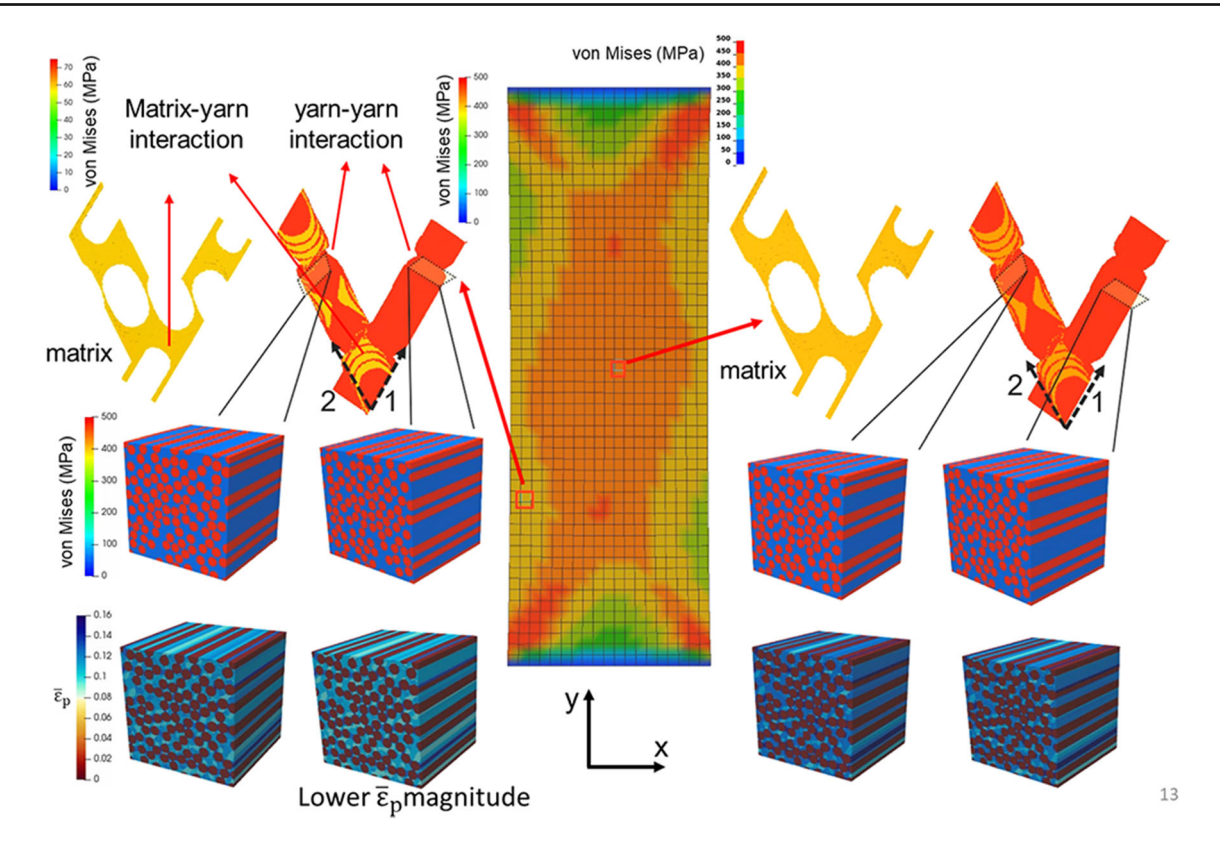


Fig. 11 Visualization at axial strain of 0.016: Cured woven bias-extension sample von Mises stress contour, mesoscale yarn and matrix von Mises stress contour, and microscale von Mises stress and effective plastic strain contours

laminate under 3-point bending and cured woven bias extension test. The proposed concurrent multiscale theory captured the extra plasticity in the mesoscale woven RVE yarn phase by modeling the varn with microscale UD RVEs. Without accounting for the extra plastic deformation in the yarn phase, the force-axial strain curve predicted by the 2-scale model diverges far away from the test data. The 3-scale model, on the other hand, is able to capture the correct trend of the loading force history with reasonable accuracy. On top of that, by modeling the yarn phase with UD RVEs at different fiber volume fractions, the upper and lower bounds of the force-strain curve can be captured. This makes the 3-scale model a powerful tool for modeling woven composite structures with the consideration of the fabrication tolerance in the UD fiber volume fraction. Such capability can help build a better understanding of the woven structural performance, accelerating the search for the optimal composite fiber volume fraction in the woven composite structure by avoiding excessive experimental trial and error. In the future, failure criteria for the 3-scale models can be added to expand the capability of the concurrent modeling theory in predicting failure behavior, such as composite delamination.

**Supplementary Information** The online version contains supplementary material available at https://doi.org/10.1007/s00466-022-02199-2.

**Acknowledgements** The financial support for this work was provided by AFOSR (FA9550-18-1-0381) and National Science Foundation's Mechanics of Materials and Structures (MOMS) program under the Grant No. MOMS/CMMI-1762035.

## Appendix A: Formulation of the reduced order modeling method

The reduced order modeling method utilized the incremental form of the Lippmann-Schwinger equation given in Eq. A.1, of which the FFT method was based on.

$$\Delta \varepsilon(x) = \Delta \varepsilon^{M} - \int_{\Omega} \mathbf{\Gamma}^{0}(x, x') : (\Delta \sigma(x'))$$
$$-\mathbf{C}^{0} : \Delta \varepsilon(x')) dx'$$
(A.1)

where  $\Delta \varepsilon(x)$  is the RVE voxel-wise incremental strain tensor,  $\Delta \sigma(x)$  is the RVE voxel-wise incremental stress tensor,  $C^0$  is the stiffness tensor of the elastic reference material, and  $\Gamma^0$  is the isotropic Green's function based on reference material  $C^0$ , x represents integration point within each cluster.  $\Delta \varepsilon^M$  is the strain increment passed in from the macroscale calculation. Note that the stress tensor at each integration point can be computed using elastic and elasto-platic material laws. In this work, isotropic elasticity, transversely isotropic



elasticity, and J2 plasticity are used to evaluate the stress tensor at each integration point.

For each RVE, assuming its voxels can be classified into a limited number of clusters, where each cluster share the same strain and stress increment, it is possible to arrive at the following discretized Lippmann-Schwinger equation in Eq. A.2

$$\frac{1}{c^{I}|\Omega|} \int_{\Omega} \chi^{I}(\mathbf{x}) \Delta \boldsymbol{\varepsilon}(\mathbf{x}) d\mathbf{x} = \Delta \boldsymbol{\varepsilon}^{M} 
- \frac{1}{c^{I}|\Omega|} \int_{\Omega} \int_{\Omega} \chi^{I}(\mathbf{x}) \boldsymbol{\Gamma}^{\mathbf{0}}(\mathbf{x}, \mathbf{x}') : (\Delta \boldsymbol{\sigma}(\mathbf{x}') 
- \boldsymbol{C}^{0} : \Delta \boldsymbol{\varepsilon}(\mathbf{x}') d\mathbf{x}' d\mathbf{x}$$
(A.2)

where  $|\Omega|^I$  is the domain volume of cluster I,  $c^I$  is the volume fraction of cluster I in the RVE domain, and  $|\Omega|$  is the RVE domain volume. The  $\chi(x)$  function equals 1 when x is in the cluster I, otherwise it will be 0. This allows one to further simplify the discretized Lippmann-Schwinger equation to Eq. A.3

$$\Delta \varepsilon^{I} = \Delta \varepsilon^{M} - \sum_{J=1}^{K} \left[ \frac{1}{c^{I} |\Omega|} \int_{\Omega} \int_{\Omega} \chi^{I}(x) \chi^{J}(x') \Gamma^{0}(x, x') dx' dx : (\Delta \sigma^{J} - C^{0} : \Delta \varepsilon^{J}) \right]$$
(A.3)

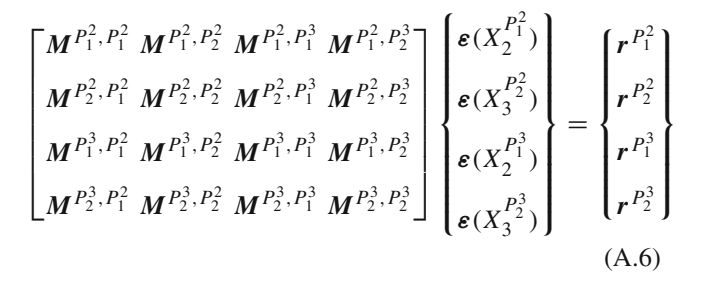
One should notice that in Eq. A.3, the Green's function can be separated out, forming a constant interaction tensor for the ROM. The interaction tensor is defined in Eq. A.4

$$\mathbf{D}^{IJ} = \frac{1}{c^I |\Omega|} \int_{\Omega} \int_{\Omega} \chi^I(\mathbf{x}) \chi^J(\mathbf{x}') \Gamma^{\mathbf{0}}(\mathbf{x}, \mathbf{x}') d\mathbf{x}' d\mathbf{x}$$
(A.4)

Finally, the discretized Lippmann-Schwinger equation can be written as Eq. A.5, which can be solved with Newton's method. Comparing Eq. A.5 to Eq. A.1, only *K* strain tensors needs to be evaluated, and *K* is much less than the number of voxels in the original RVE. Therefore, the ROM can significantly reduce the overall computational cost of the 3-scale concurrent model, while allowing one to track the RVE strain and stress evolution.

$$\Delta \boldsymbol{\varepsilon}^{I} = \Delta \boldsymbol{\varepsilon}^{M} - \sum_{J=1}^{K} \left[ \boldsymbol{D}^{IJ} : (\Delta \boldsymbol{\sigma}^{J} - \boldsymbol{C}^{0} : \Delta \boldsymbol{\varepsilon}^{J}) \right]$$
 (A.5)

To solve the lower-scales a multiresolution clustering analysis [22] approach can be adopted. Interested readers can find the details of the multiresolution clustering analysis formulation by Yu et al. [22] which has the following matrix form for the lower two scales.



where M is the Jacobian matrix and  $P_i^j$  means the phase i, of scale j. For example, for a three-scale woven composite, scale 1 is the macro-scale, scale 2 in the woven scale and scale 3 is the UD scale. For woven scale 2, the matrix phase is denoted by  $P_1^2$ , and the yarn phase is denoted by  $P_2^2$ . For UD scale 3, the matrix phase is denoted by  $P_1^3$ , and the fiber phase is denoted by  $P_2^2$ .  $\varepsilon$  and r are the strain and the residual matrix, respectively.

# Appendix B: Concurrent stress evolution in three-point bending test of woven laminate

In Fig. 12 a) to c) the von Mises stress fields evolution for the macroscale woven laminate, mesoscale woven microstructures, and microscale UD microstructures are visualized. Fig. 12 a), b), and c) are taken at impactor displacements of 0.16 mm, 0.32 mm, and 0.48 mm, respectively. Note that woven RVEs for all 6 plies (through the thickness), at the outermost region in the middle of the woven laminate, are plotted. The two UD RVEs depicted represent two yarns, one in the first ply and one in the third ply.

As the impactor gradually bends the laminate, the von Mises stress magnitude of the laminate increases. To be specific, the top and bottom layer are experiencing compression and tension stresses, respectively. The neutral surface of the laminate, which is between the third and fourth ply, shows very little increase in von Mises stress, as expected. Fig. 12 shows the von Mises stress of the top and bottom layer increasing rapidly, whereas plies in the middle experience a very small increase. For further illustration, the yarn microstructure responses are captured by UD RVEs. The fiber phase in the UD RVE representing the yarn in the first woven ply experiences a much higher increase in von Mises stress magnitude, whereas the fiber phase in the third ply bares much less stress. The laminate bending causes bending stress along the x direction of the laminate, which coincides with the 1 direction in the yarn. Therefore, one can see at the mesoscale, yarns in the 1 direction are the primary load-carrying constituents. As the yarn responses are approximated by the UD RVE, and the UD fiber direction coincides with the woven 1 direction, the fiber phase in the UD RVE carries the load, as expected. Therefore, aforementioned evolution of the von Mises stress across all three



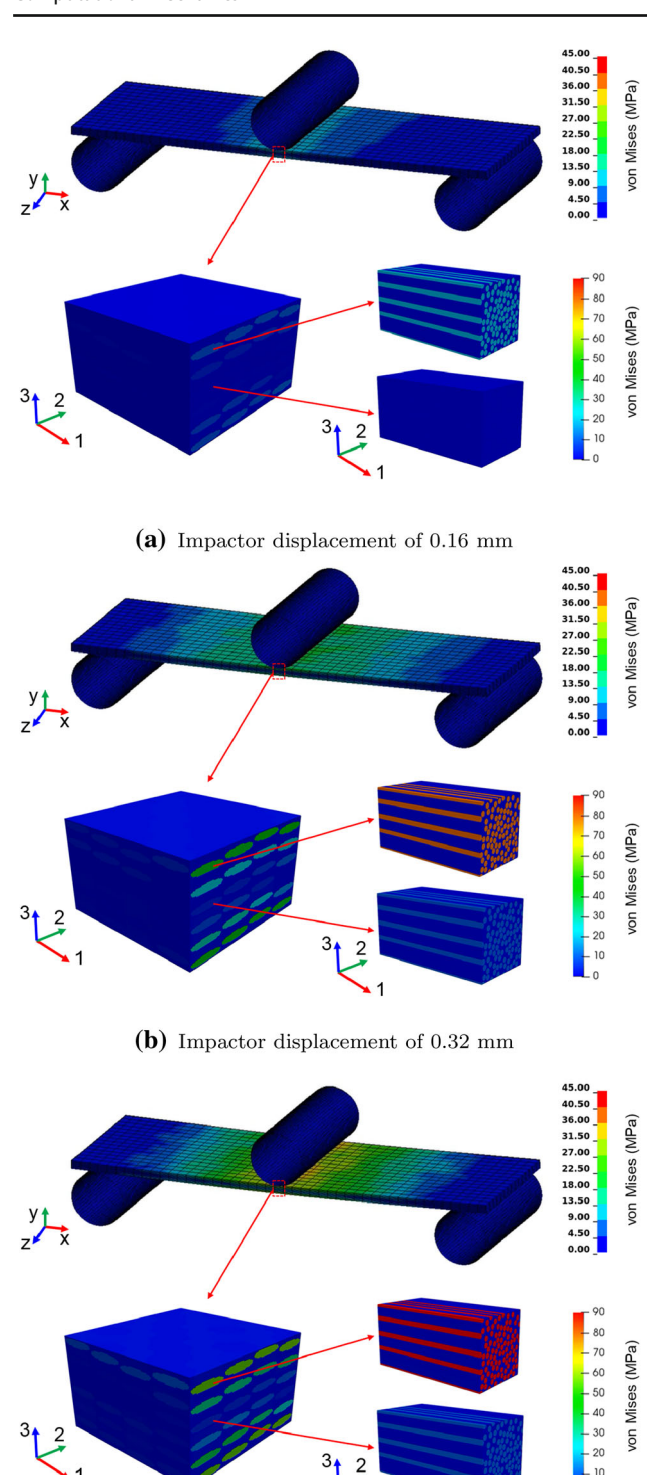


Fig. 12 Three snapshots to illustrate the macroscale (woven laminate), mesocale (woven RVEs) and microscale (UD RVEs) stress evolution

(c) Impactor displacement of 0.48 mm

scales is physical, and it reveals underneath microstructure evolution in the woven laminate structure only enabled by the 3-scale concurrent modeling.

#### References

- Kari S, Berger H, Gabbert U (2007) Numerical evaluation of effective material properties of randomly distributed short cylindrical fibre composites. Comput Mater Sci 39(1 SPEC. ISS.):198–204. https://doi.org/10.1016/j.commatsci.2006.02.024
- Bradshaw RD, Fisher FT, Brinson LC (2003) Fiber waviness in nanotube-reinforced polymer composites-II: Modeling via numerical approximation of the dilute strain concentration tensor. Compos Sci Technol 63(11):1705–1722. https://doi.org/10.1016/S0266-3538(03)00070-8
- Liang B, Zhang W, Fenner JS, Gao J, Shi Y, Zeng D, Su X, Liu WK, Cao J (2019) Multi-scale modeling of mechanical behavior of cured woven textile composites accounting for the influence of yarn angle variation. Compos A Appl Sci Manuf 124:105460. https://doi.org/10.1016/j.compositesa.2019.05.028
- Gao J, Liang B, Zhang W, Liu Z, Cheng P, Bostanabad R, Cao J, Chen W, Liu WK, Su X et al (2017) Multiscale modeling of carbon fiber reinforced polymer (cfrp) for integrated computational materials engineering process. Tech. rep, Ford Motor Company
- Sun Q, Guo H, Zhou G, Meng Z, Chen Z, Kang H, Keten S, Su X (2018) Experimental and computational analysis of failure mechanisms in unidirectional carbon fiber reinforced polymer laminates under longitudinal compression loading. Compos Struct 203:335

  348. https://doi.org/10.1016/j.compstruct.2018.06.028
- Sun Q, Zhou G, Meng Z, Guo H, Chen Z, Liu H, Kang H, Keten S, Su X (2019) Failure criteria of unidirectional carbon fiber reinforced polymer composites informed by a computational micromechanics model. Compos Sci Technol 172:81–95. https:// doi.org/10.1016/j.compscitech.2019.01.012
- Li H, Kafka OL, Gao J, Yu C, Nie Y, Zhang L, Tajdari M, Tang S, Guo X, Li G et al (2019) Clustering discretization methods for generation of material performance databases in machine learning and design optimization. Comput Mech 64(2):281–305
- He C, Ge J, Zhang B, Gao J, Zhong S, Liu WK, Fang D (2020) A hierarchical multiscale model for the elastic-plastic damage behavior of 3d braided composites at high temperature. Composites Science and Technology 108230
- Liu Y, Straumit I, Vasiukov D, Lomov SV, Panier S Multi-scale material model for 3D composite using Micro CT Images geometry reconstruction, ECCM 2016 - Proceeding of the 17th European Conference on Composite Materials (June)
- Dasgupta A, Agarwal RK, Bhandarkar SM (1996) Threedimensional modeling of woven-fabric composites for effective thermo-mechanical and thermal properties 3538(95):209–223
- Liang B, Zhang W, Fenner JS, Gao J, Shi Y, Zeng D, Su X, Liu WK, Cao J (2019) Multi-scale modeling of mechanical behavior of cured woven textile composites accounting for the influence of yarn angle variation. Compos A Appl Sci Manuf 124:105460
- Bostanabad R, Liang B, Gao J, Liu WK, Cao J, Zeng D, Su X, Xu H, Li Y, Chen W (2018) Uncertainty quantification in multiscale simulation of woven fiber composites. Comput Methods Appl Mech Eng 338:506–532
- He C, Ge J, Qi D, Gao J, Chen Y, Liang J, Fang D (2019) A multiscale elasto-plastic damage model for the nonlinear behavior of 3d braided composites. Compos Sci Technol 171:21–33
- Liu Z, Bessa M, Liu WK (2016) Self-consistent clustering analysis: an efficient multi-scale scheme for inelastic heterogeneous materials. Comput Methods Appl Mech Eng 306:319–341
- Liu Z, Fleming M, Liu WK (2018) Microstructural material database for self-consistent clustering analysis of elastoplastic strain softening materials. Comput Methods Appl Mech Eng 330:547–577
- Yuan Z, Fish J (2008) Toward realization of computational homogenization in practice. Int J Numer Meth Eng 73(3):361–380



- Wulfinghoff S, Cavaliere F, Reese S (2018) Model order reduction of nonlinear homogenization problems using a hashin-shtrikman type finite element method. Comput Methods Appl Mech Eng 330:149–179
- Han X, Gao J, Fleming M, Xu C, Xie W, Meng S, Liu WK (2020) Efficient multiscale modeling for woven composites based on selfconsistent clustering analysis. Comput Methods Appl Mech Eng 364:112929
- Gao J, Shakoor M, Domel G, Merzkirch M, Zhou G, Zeng D, Su X, Liu WK (2020) Predictive multiscale modeling for unidirectional carbon fiber reinforced polymers. Compos Sci Technol 186:107922
- Gao Z, Chen L (2021) A review of multi-scale numerical modeling of three-dimensional woven fabric. Transactions of the Metallurgical Society of AIME 263:113685
- Standard A (2013) D792-13, 2013, "standard test methods for density and specific gravity (relative density) of plastics by displacement"in: Astm international, west conshohocken https://doi. org/10.1520/d0792-13
- Yu C, Kafka OL, Liu WK (2021) Multiresolution clustering analysis for efficient modeling of hierarchical material systems. Comput Mech 67(5):1293–1306
- Jacob F, Ted B (2007) A first course in finite elements. Wiley, Newyork
- Hughes TJ (2012) The finite element method: linear static and dynamic finite element analysis. Courier Corporation, North Chelmsford, Massachusetts, p 2012
- Belytschko T, Liu WK, Moran B, Elkhodary K (2014) Nonlinear finite elements for continua and structures. John wiley & sons, Newyork
- Hughes TJ, Cottrell JA, Bazilevs Y (2005) Isogeometric analysis:
   Cad, finite elements, nurbs, exact geometry and mesh refinement.
   Comput Methods Appl Mech Eng 194(39–41):4135–4195
- Cottrell JA, Hughes TJ, Bazilevs Y (2009) Isogeometric analysis: toward integration of CAD and FEA. John Wiley & Sons, Newyork
- 28. Belytschko T, Lu YY, Gu L (1994) Element-free galerkin methods. Int J Numer Meth Eng 37(2):229–256
- Liu WK, Jun S, Zhang YF (1995) Reproducing kernel particle methods. Int J Numer Meth Fluids 20(8–9):1081–1106
- Li S, Liu WK (2002) Meshfree and particle methods and their applications. Appl Mech Rev 55(1):1–34
- Goldberg R, Carney KS, DuBois P, Hoffarth C, Harrington J, Rajan S, Blankenhorn G (2014) Theoretical development of an orthotropic elasto-plastic generalized composite material model. National Aeronautics and Space Administration, Glenn Research Center

- 32. Khashaba U, Seif M (2006) Effect of different loading conditions on the mechanical behavior of [0/±45/90] s woven composites. Compos Struct 74(4):440–448
- Ullah H, Harland AR, Silberschmidt VV (2012) Damage modelling in woven-fabric cfrp laminates under large-deflection bending. Comput Mater Sci 64:130–135
- Gao J, Shakoor M, Jinnai H, Kadowaki H, Seta E, Liu, WK (2019)
   An inverse modeling approach for predicting filled rubber performance. Comput Methods Appl Mech Eng 357:12567
- Zweben C, Smith W, Wardle M (1979) Test methods for fiber tensile strength, composite flexural modulus, and properties of fabricreinforced laminates, in: Composite Materials: Testing and Design (Fifth Conference), ASTM International
- Hollomon H (1945) Tensile deformation. Transactions of the Metallurgical Society of AIME 162:268–290
- Sun Q, Meng Z, Zhou G, Lin S-P, Kang H, Keten S, Guo H, Su X (2018) Multi-scale computational analysis of unidirectional carbon fiber reinforced polymer composites under various loading conditions. Compos Struct 196:30–43. https://doi.org/10.1016/j.compstruct.2018.05.025
- 38. Long A, Brown L (2011) Modelling the geometry of textile reinforcements for composites: Texgen, in: Composite reinforcements for optimum performance, Elsevier, pp. 239–264
- Manual L-DKU (2007) Volume I Version 971. Livermore Software Technology Corporation 7374:354

**Publisher's Note** Springer Nature remains neutral with regard to jurisdictional claims in published maps and institutional affiliations.

